

An Efficient Electrocatalyst based on Platinum Incorporated into N,S co-doped Porous Graphene for Oxygen Reduction Reaction in Microbial Fuel Cell

S. Sadegh Hassani¹, M.R. Ganjali^{1,2,}, L. Samiee³ and A.M. Rashidi⁴*

¹ Center of Excellence in Electrochemistry, School of Chemistry, College of Science, University of Tehran, Tehran, Iran

² Biosensor Research Center, Endocrinology and Metabolism Molecular-Cellular Sciences Institute, Tehran University of Medical Sciences, Tehran, Iran

³ Energy Technology Research Division, Research Institute of Petroleum Industry (RIPI), West Blvd. Azadi Sport Complex, P.O. Box 14665-137, Tehran, Iran

⁴ Nanotechnology Research Center, Research Institute of Petroleum Industry (RIPI), West Blvd. Azadi Sport Complex, P.O. Box 14665-137, Tehran, Iran

*E-mail: ganjali@khayam.ut.ac.ir

Received: 10 August 2018 / *Accepted:* 21 September 2018 / *Published:* 1 October 2018

In this work, an efficient electrocatalyst nanomaterial for application in fuel cells was introduced. The nanomaterial was prepared through platinum incorporation into the S,N co-doped porous graphene (PG) through pyrolysis method. The physico-chemical properties of the prepared samples were characterized using X-ray Diffraction (XRD), Raman spectroscopy, N₂ sorption-desorption, Transmission Electron Microscopy (TEM), Field Emission Scanning Electron Microscopy (FESEM) and X-ray Photoelectron Spectroscopy (XPS). The synthesized samples were further applied for oxygen reduction reaction (ORR) and evaluation in microbial fuel cell (MFC). The results revealed that impregnation of 10 wt.% Pt into the nitrogen and sulfur co-doped graphene structure (called G-STP-900-Pt 10) cause more improvement in catalytic activity compared to 20 wt.% Pt/C. Also, LSV measurements confirmed an improved onset potential (1.00 V) for G-STP-900-Pt 10 sample in comparison with 20 wt.% Pt/C (0.99 V vs. RHE). Furthermore, microbial fuel cell test showed higher cell potential and power density relative to Pt/C 20 wt.% too. Finally, for economic purpose, the optimal sample with lower Pt amount (10 wt.% Pt) was selected as a good candidate for ORR in MFCs.

Keywords: Oxygen reduction reaction, Microbial fuel cell, Porous graphene, Platinum, Nitrogen and sulfur co-doped graphene.

1. INTRODUCTION

Cathode electrocatalyst has an important role for oxygen reduction reaction (ORR) in some devices such as Fuel cells and metal-air batteries for clean energy production. Platinum based catalysts because of their high efficiency has been intensively applied in designing fuel cells [1-2].

However, platinum cost, low abundance and the sluggish oxygen reduction reaction (ORR) cause some significant limitations in fuel cell efficiency. Several researches have been made to resolve these problems, by reducing electrocatalysts cost and improving activity of oxygen reduction reaction (ORR). In this regards, some strategies such as using lower noble metals content [3], replacing noble metals with low price elements [4] and utilizing of metal-free electrocatalysts have been developed [5-7]. Recently, carbon based materials owing to their low cost, high stability and durability have been applied as a high efficient metal free electrocatalysts for ORR applications [8-10]. Moreover, the difference in electronegativity and bond length between heteroatoms and carbon atoms leads to an increase in electrical conductivity and electrochemical activity of the heteroatom doped carbon materials. These materials have been used as cathode electrocatalyst for the ORR [11-13]. The hetero-atom doped carbon materials with low cost and enhanced electrical conductivity can be also good candidates for using as the ORR support [14-16]. In addition, Pt as the most promising electrochemical metal has been used to facilitate the oxygen reduction reaction from the last decades. Therefore, Pt impregnation on the heteroatom doped carbon materials could lead to reducing the required Pt amount for achievement of high ORR activity.

In the work presented here, for the first time, an efficient electrocatalyst nanomaterial for application in fuel cells was introduced. The used nanomaterial was a low amount of platinum incorporated into a S,N co-doped porous graphene (PG). The N, S co-doped porous graphene was prepared using sulfur trioxide pyridine complex (STP) via pyrolysis method and the electrocatalytic performances of the doped graphene sample for oxidation reduction reaction in alkaline media and microbial fuel cell was studied. The results were then compared with the PG and Pt/C 20 wt.%. In this regards, the optimum amount of Pt on PG was selected for impregnation of Pt on the N, S co-doped porous graphene. The prepared electrocatalysts showed high selectivity toward four-electron reduction pathway and almost higher onset potential with lower amount of Pt compared to commercial Pt/C 20wt.% catalysts. The microbial fuel cell results showed the optimal catalyst has a promising performance in relation to the Pt/C 20wt.% commercial catalyst due to the synergistic effect of N and S atoms with specific structures (e.g. C–S–C and pyridinic-N) in the graphene structure.

2. EXPERIMENTAL

2.1. Materials and reagents

Chloroplatinic acid hexahydrate, Sulfur trioxide pyridine complex, KOH, HCl (37%), Ethanol (99.8%), Nafion (5 wt% in lower aliphatic alcohols and water) and Pt 20wt.% on Vulcan XC72 were purchased from Sigma-Aldrich Company.

2.2. Synthesis of samples

2.2.1. Synthesis of heteroatom doped graphene

Porous graphene (PG) was synthesized and purified according to the method described in our previous paper [10, 18]. Preparation of heteroatom doped graphene sample using sulfur trioxide pyridine complex precursor was done according to the previously reported work [19]. Sulfur trioxide pyridine complex solution was added to a dispersion of PG in ethanol under stirring. The mixture was dried and pyrolyzed at 900°C for 2 h in N₂ atmosphere. The prepared sample will be referred as G-STP 900, which was applied as supporting material for impregnation of platinum.

2.2.2. Impregnation of Pt on the graphene structures

0.1 g of graphene was poured into 60 ml of ethanol solution, and the resulting mixture was stirred at room temperature for 30 min using a magnetic stirrer at a rate of 500 rpm. Chloroplatinic acid hexahydrate solution was dissolved in 10 ml of ethanol and added to the previous mixture to prepare 5, 10 and 20 wt. % of platinum on graphene. The resulting mixture was then stirred at room temperature for 1 hour at 500 rpm, dried under atmospheric nitrogen at room temperature and reduced at 350°C in hydrogen flow for 5 hours. Platinum was impregnated on the PG with different ratios of 5, 10 and 20wt.% and named as PG-Pt-5, PG-Pt-10 and PG-Pt-20, respectively. The synthesis of Pt on the prepared heteroatom doped graphene (G-STP 900) in section 2.2.1 was done in a similar procedure using Pt 10wt.%, and the synthesized catalyst was named as G-STP 900-Pt 10.

2.3. Characterizations techniques

The X-ray diffraction instrument 10-80° (a Kemiatic DX-27 device using CuK_α, $k=0.154$ nm, radiation) was used to characterize the samples structures. A Field emission scanning electron microscope (Mira-TSCAN), equipped with Energy Dispersive Spectroscopy (EDS) was applied to obtain the samples morphology and map analysis. In addition, the TEM image was obtained with Tecnai G2 F20 S TWIN HR(S) TEM, FEI. The nitrogen adsorption/desorption isotherms were obtained at 77 K with a micromeritics Tristar 3000 apparatus, while the sample degassing was done at 373K for 4 h before to analysis. An Almega Thermo Nicolet with an Ar ion laser source with excitation wavelength of 514 nm was applied for Raman measurements. The surface chemical composition was investigated using an X-ray photoelectron spectroscopy (XPS), using a Physical Electronics Model 5700 XPS instrument, which was equipped with a monochromatic Al-K_α X-ray source (1486.6eV) operating at 350 W.

2.4. Electrochemical measurements

An Autolab potentiostat/galvanostat PGSTAT30 electrochemical workstation equipped three-electrode cell was used for electrochemical measurements. A platinum and Ag/AgCl saturated with

KCl were used as the counter and reference electrodes, respectively. The KOH 0.1 M solution was saturated with oxygen for 1 hour before the analysis applied as electrolyte. The electrocatalytic activity towards ORR was measured in O₂-saturated 0.1 M KOH solution by. Linear sweep voltammetry (LSV) at a scan rate of 5mV/s using a rotating disk electrode was performed at various rotation speeds from 250 to 3500 rpm. Cyclic voltammetry (CV) was measured within a voltage range from -0.03 to 1.16 V (vs. RHE electrode) at a scan rate of 50mV/s. The electron transfer number was calculated using the Koutecky–Levich equation [19, 20]. Moreover, chronoamperometry analysis was used for electrodes stability evaluation. The working electrode was prepared using a 5 mg mL⁻¹ solution of catalyst ink in ethanol–water solution (1:1) including Nafion solution (20 wt.% in ethanol), coated on (GC) electrode and dried in air at 60°C. The total catalyst loading on the GC electrode was calculated to be 0.3 mg cm⁻².

2.5. Microbial Fuel cell test (MFC) measurement

Cubic-shaped MFC was used for evaluating the synthesized samples. The anodic and cathodic chambers of the constructed MFCs were separated using a CMI-7000 cation exchange membrane and the chambers were sealed together by a gasket. The anodic chamber was filled with 0.31 g NH₄Cl and 0.5 ml vitamin B complex solution in phosphate buffer (20 mM, pH 7.2) per liter of deionized water and the cathode chamber filled with phosphate buffer solution (50 mM, pH 7.2). An aerobic activated sludge was obtained from industrial wastewater treatment plant of Research Institute of Petroleum Industry (RIPI), Tehran, Iran and cultured in the anodic chamber while 700 ppm phenol solution (flow rate 100 µl/min) was fed continuously to this chamber as the sole carbon and energy source [21]. The anode electrode material was heat-treated carbon graphite brush and the cathode electrode was carbon paper with heteroatom doped graphene catalyst on the water facing side. 23.7 mg heteroatom doped graphene catalyst was coated on 9.0 cm² of the cathode surface area which was covered with four PTFE (Polytetrafluoroethylene) diffusion layers on the air side. A copper wire was used to connect the electrodes using a 1,000 Ω resistor. All the experiments were conducted in temperature-controlled conditions at 25°C.

3. RESULTS AND DISCUSSION

3.1. Structural Characterization

Fig. 1 shows XRD pattern of PG, G-STP-900 samples, which a peak in 2θ equal 25.1° is related to the (002) graphite structure reflection. According to the XRD results, the peak at (002) is positively shifted toward higher degrees and an asymmetry observed at the peak (002) of doped sample, due to increasing defects in graphene structure created by nitrogen and sulfur doping under pyrolysis of PG in presence of heteroatom precursors at high temperature [22].

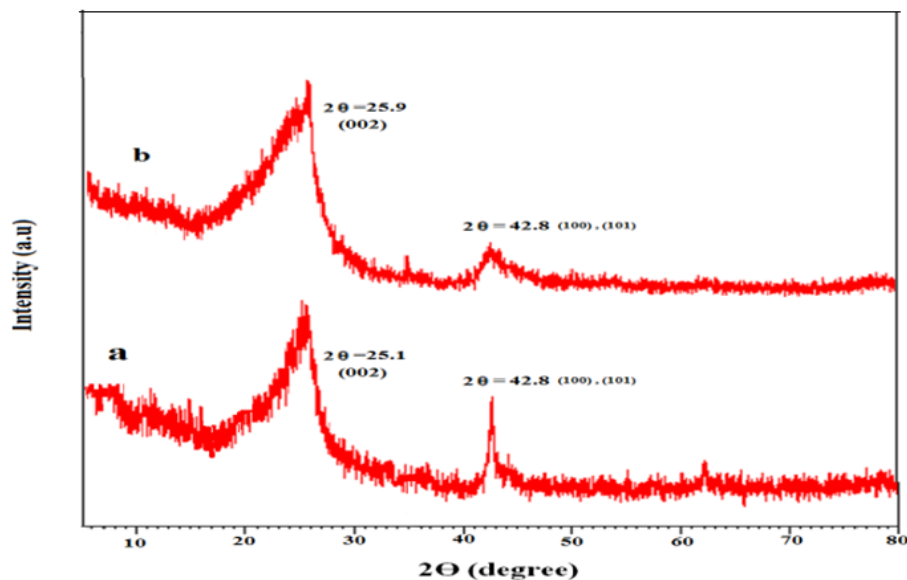


Figure 1. XRD pattern of a: PG b: G-STP- 900

The defects level as a result of dopant atom incorporation in the graphene was studied using Raman spectroscopy [23-24]. The main peaks in Raman spectrum for Graphene are G ($\sim 1580\text{ cm}^{-1}$), D ($\sim 1350\text{ cm}^{-1}$) and 2D ($\sim 2680\text{ cm}^{-1}$), which D band is related to defects, disordered sp^2 carbon atoms or entered heteroatoms into structure. The peak at 2950 cm^{-1} associated with a D + G combination mode induced by defects. The peak at 2400 cm^{-1} indicates N_2 gas present in the air surrounding the sample [19, 25-27].

Fig. 2 shows Raman spectrum of PG, G-STP-900 samples. The D and G band intensities ratio shows carbon structure disordering and heteroatom doping. The higher value of I_D/I_G is indicative of more defects and presence of heteroatom in graphene structure [19, 28]. The I_D/I_G values for PG and G-STP-900 samples are calculated and presented in Table 1 showing the G-STP-900 sample has higher amount (1.17) compared to PG (0.96). The higher I_D/I_G ratio for the G-STP-900 sample could be related to heteroatoms doping in sample, high level of defects and structural disordering that cause the improved oxygen adsorption.

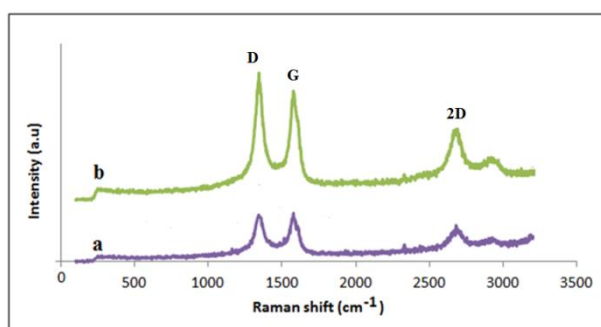


Figure 2. Raman spectra of (a) PG, (b) G-STP- 900

Table 1. Raman specification of the PG and G-STP-900 samples

Sample	G band (cm ⁻¹)	D band (cm ⁻¹)	2D band (cm ⁻¹)	I _D	I _G	I _D /I _G
PG	1577.2	1341.85	2681.17	282.84	294.63	0.96
G-STP-900	1577.12	1343.99	2679.13	770.18	660.58	1.17

According to the adsorption-desorption isotherms of PG and G-STP-900 samples, the textural parameters such as: BET specific surface area, pore volume and pore diameter were obtained and presented in Table 2.

Table 2. Textural parameters of the PG and G-STP-900 samples

Sample	BET Surface Area (m ² g ⁻¹)	Pore Volume (cm ³ g ⁻¹)	Mean Pore Size (nm)
PG	629.3	2.03	12.9
G-STP-900	178.7	0.44	9.7

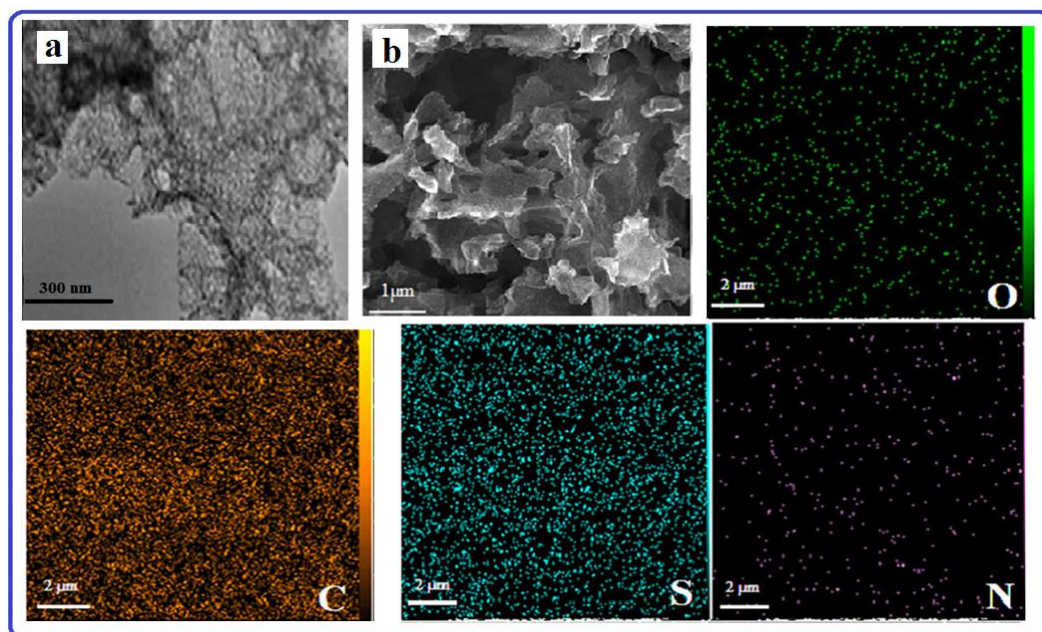


Figure 3. (a) TEM image of PG, (b) FESEM image of G-STP-900 sample; EDX mapping analysis of N, C, S and O elements in the G-STP-900

The porous structure of PG with average pore size around 12.9 nm and graphene nanosheets are presented in TEM image (Fig. 3a). Furthermore, the surface morphology of the G-STP-900 was observed by Field emission scanning electron microscope (FESEM) shown in Fig. 3b.

Moreover, the EDX image mapping analysis of the G-STP-900 sample in Fig. 3 exhibited good and uniform dispersion of nitrogen, sulfur and oxygen in the carbon structure confirming that N and S have been successfully doped in graphene.

In addition, X-ray photoelectron spectroscopy (XPS) spectrum over a wide range of binding energies (0-1400 eV) is used to investigate nitrogen and sulfur atoms in G-STP-900 structure, showing graphitic C 1s (284.4 eV), O 1s (~530 eV), N 1s (~400 eV) and S 2P (~165 eV) peaks (Fig. 4). The high resolution XPS spectra of the N peak in G-STP-900 sample showed N-pyridinic (~398.5 eV) and N-pyrrolic (~400.6 eV) and pyridinic N-oxide (~403.2 eV) species with a nominal nitrogen level of 2% at a ratio of 60, 35% and 5%, respectively (Fig. 4). N-pyridinic was proposed to be the highly catalytic sites to facilitate the ORR process and improve the onset potential due to donation of one extra electron to the aromatic ring [19, 12, 29]. Also, the high resolution XPS spectra of the S peak in G-STP-900 sample with a 0.9% level represents the presence of C-S_n-C, C=S, sulfoxide forms in the graphene structure at the peaks around 163.8 (85%), 165.0 (10%) and 168.8 (4%), respectively [10, 12, 28].

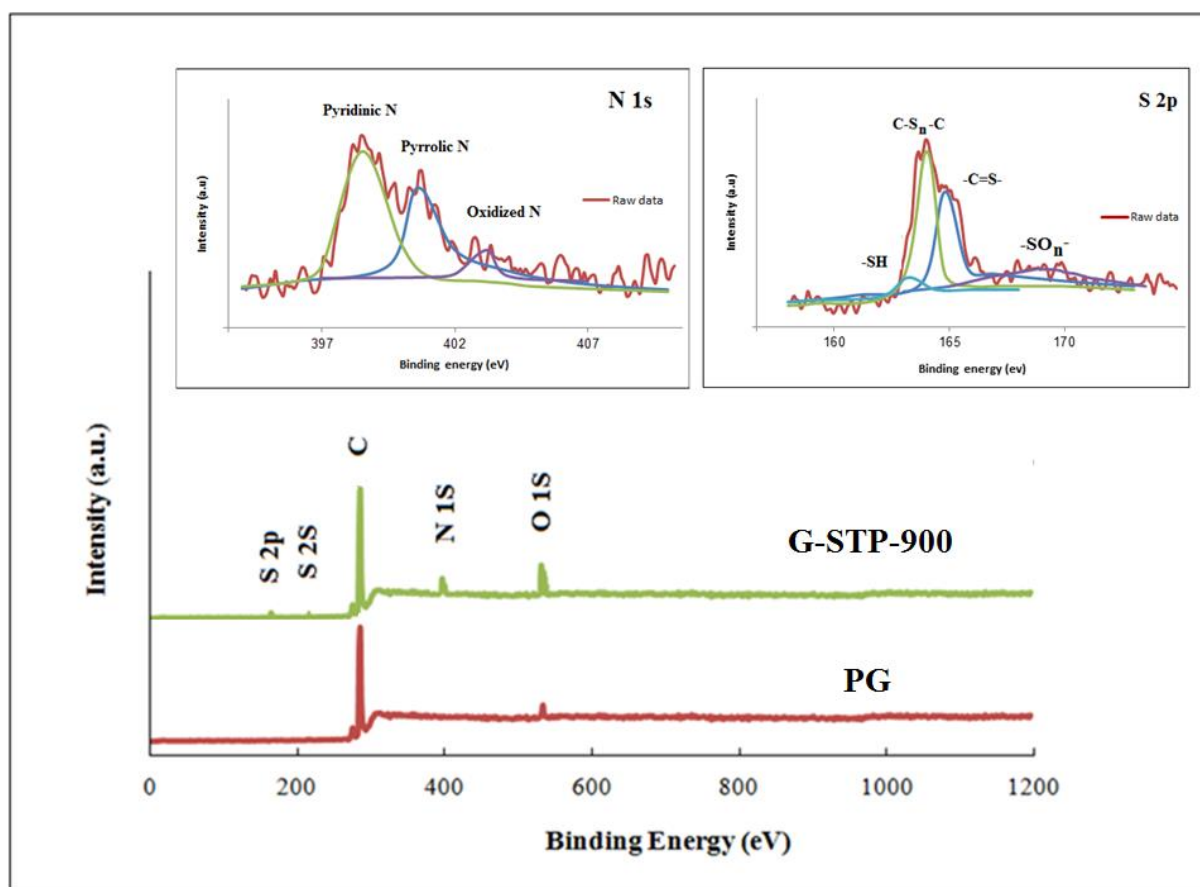


Figure 4. XPS wide spectra of PG and G-STP-900 samples, and XPS high resolution spectra of N and S in G-STP-900 sample

3.2. Electrochemical Studies

The electrocatalytic activities of the PG and G-STP-900 supports and their Platinum impregnated sample electrodes were evaluated by CV and RDE voltammetry.

3.2.1. Cyclic voltammetries

To determine the suitable amounts of platinum for impregnating on the graphene support, 5, 10 and 20% of Pt to PG were selected and impregnated on the PG support. The electrocatalysts performance was evaluated using cyclic voltammetry (CV) in an aqueous O₂ saturated 0.1 M KOH solution and compared to Pt/C (20 wt.%), shown in Fig. 5. Catalysts with higher peak current and earlier onset potential, show higher electrocatalytic activity towards the ORR.

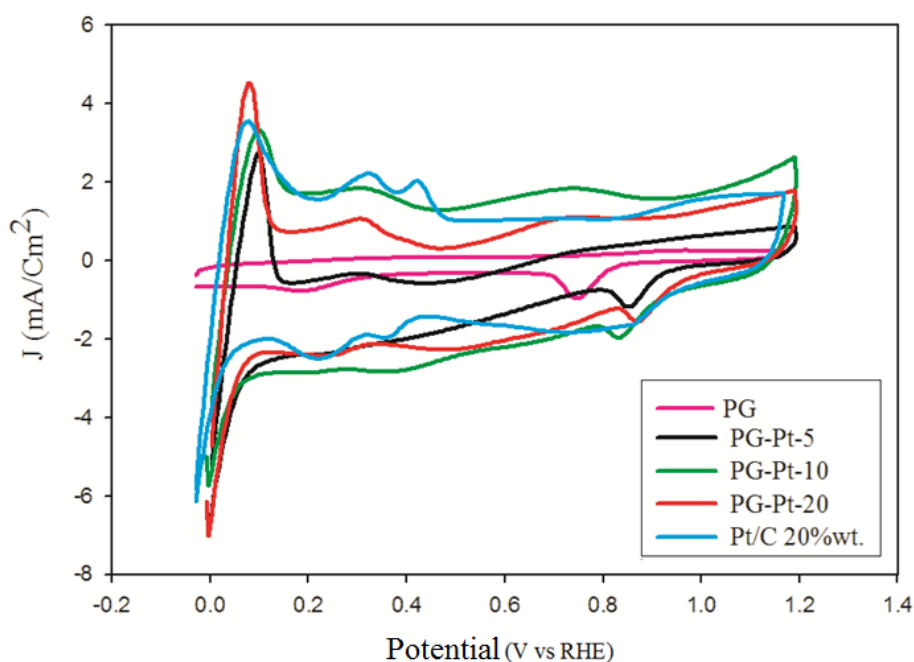


Figure 5. Cyclic voltammograms of the used electrocatalysts for oxygen reduction in O₂ saturated 0.1 M KOH at a sweep rate of 50 mV/s on the (a): 5, 10, 20% Pt impregnated on PG, bare PG and Pt/C 20 wt% electrodes

As can be seen, the onset potential of ORR for the bare PG electrode after 20 reducing CV cycles is at 0.82 V (versus RHE). The entire Pt impregnated (5, 10 and 20%) graphene samples considerably showed more positive onset potential, higher ORR reduction peak and increased current density than PG. The trend of increased potential is as: PG < PG-Pt-5 < PG-Pt-10 < Pt/C 20wt.% < PG-Pt-20, respectively. These results clearly indicate that the Pt impregnated on PG could enhance the catalytic activity relative to Pt/C 20wt.%, which among the 10% Pt is selected for impregnating on S-N doped graphene (G-STP-900).

3.2.2. Rotating Disk Electrode (RDE) test

The RDE voltammogram using a rotating disk electrode in O₂ saturated KOH 0.1 M at a scan rate of 5 mV/s was also obtained to evaluate the electrocatalytic and kinetic (Fig. 6) properties. As can be seen, the increased onset potential trend is similar to CV results.

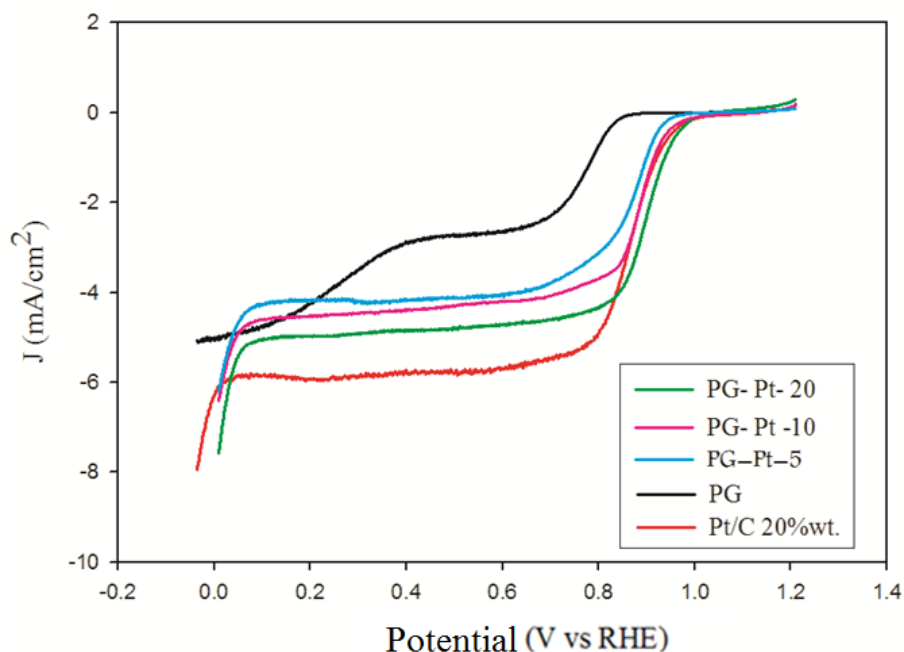
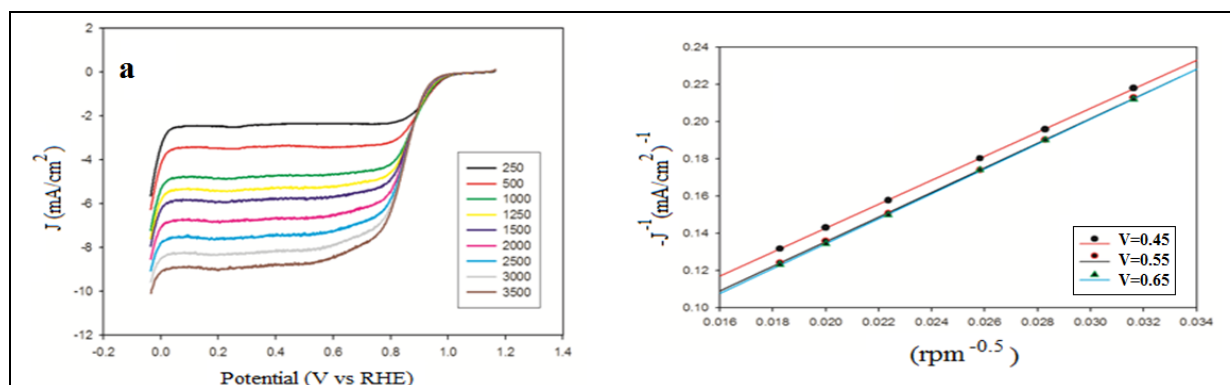


Figure 6. Comparison of linear sweep voltammetry at 1500 rpm in O₂ saturated KOH 0.1 M.

LSV curves of the prepared samples on the rotation rates from 250 to 3500 rpm were measured and electron transfer numbers (*n*) per oxygen molecule involved in the ORR process quantitatively calculated using the Koutechy–Levich equation at potentials ranging from 0.45 to 0.65 (V vs RHE) (Fig. 7).



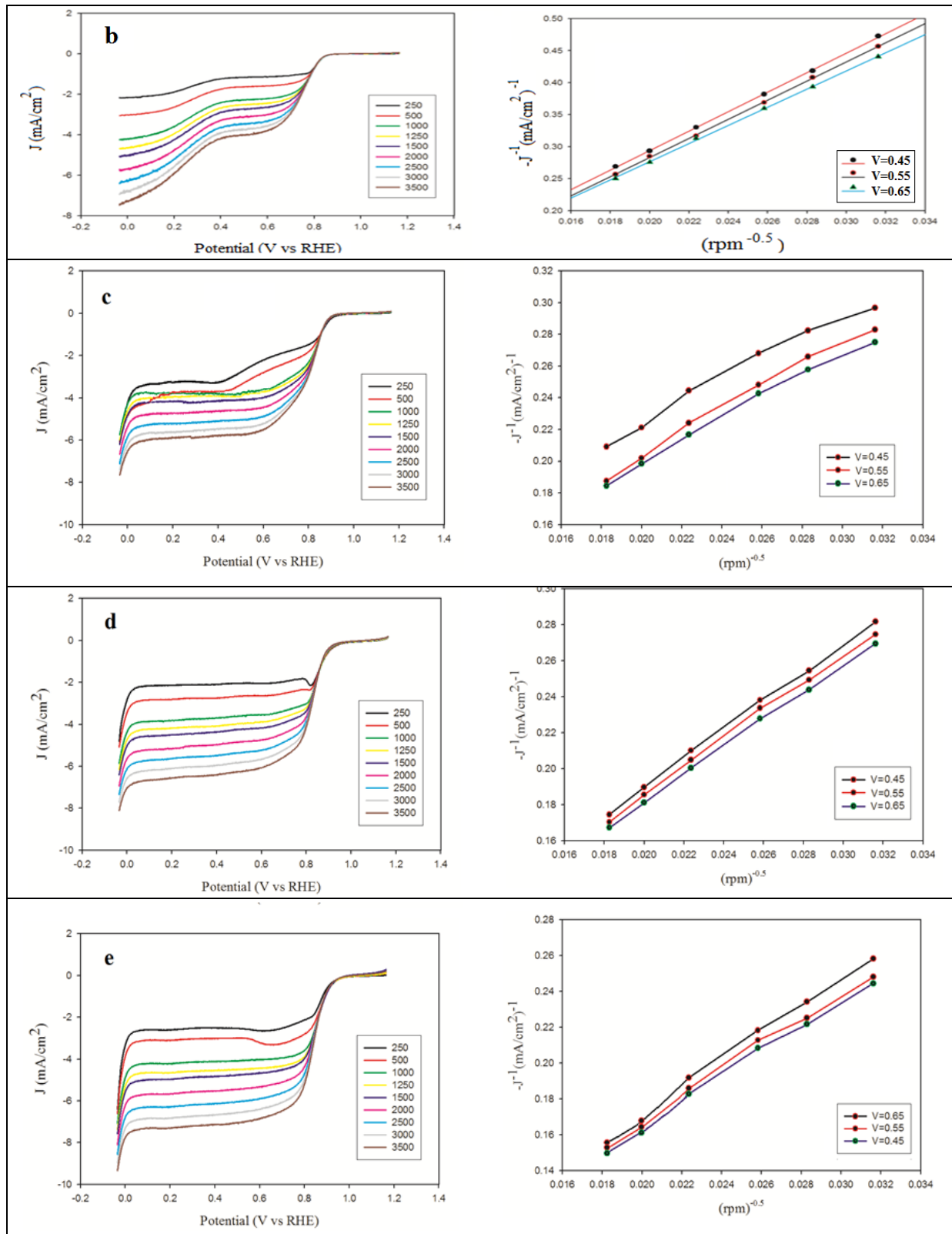


Figure 7. Linear sweep voltammetry at different rotation rate (a) PG, (b) Pt/C 20 wt%, (c) PG-Pt-5, (d) PG-Pt-10, (e) PG-Pt-20 in KOH 0.1 M (scan rate 5 mV/s). The corresponding Koutecky–Levich plots at different potentials

Table 3 shows a comparison of onset potential, electron transfer number and current density of the prepared electrocatalysts with Pt/C 20 wt.%.

Table 3. Comparison between onset potential, electron transfer number and current density of prepared electrocatalysts

Samples	Electron transfer number (n)	Onset potential (V vs. RHE)	Steady state current density (mA/cm ²)
PG-Pt-5	3.8	0.96	-4.2
PG-Pt-10	4.0	0.98	-4.6
PG-Pt-20	4.1	1.00	-5.1
PG	2.2	0.85	-5.1
Pt/C 20 wt%	4.1	0.99	-5.9

According to the obtained results, the ORR onset potential of PG is about 0.85 V (vs RHE), whereas the onset potential of Pt impregnated samples have been improved to 0.96, 0.98 and 1.00 for the PG-Pt-5, PG-Pt-10 and PG-Pt-20 samples, respectively. Despite the more appropriate onset of PG-Pt-20 sample that is higher than Pt/C 20wt.% (1.00 V vs RHE), due to economic purpose, 10 wt.% Pt sample with similar onset to Pt/C 20wt.% catalyst was selected as the optimal amount for impregnating the N,S doped graphene (G-STP-900) sample. The onset potential for the G-STP-900 electrocatalyst was 0.93 V vs. RHE which is close to the Pt/C 20wt.% (0.99 V vs RHE) [19]. Therefore, 10% Pt was impregnated on the G-STP-900 as a support and LSV measurements were performed for the G-STP-900 Pt 10 sample (Fig. 8), which confirms an improved onset potential (1.00 V vs RHE) compared to Pt/C 20wt.%.

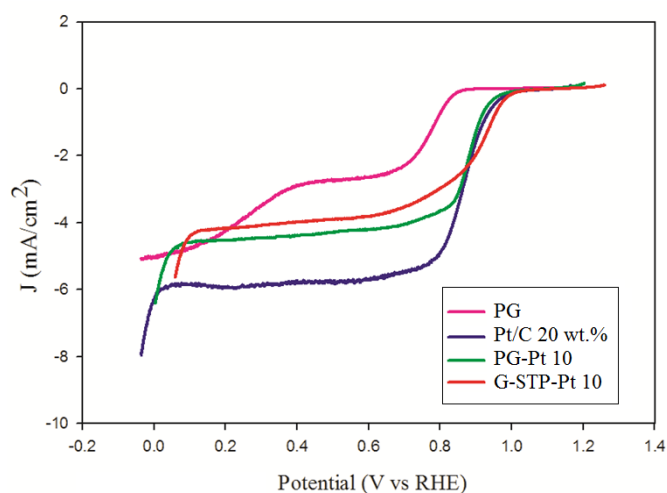


Figure 8. Linear sweep voltammetry at 1500 rpm in O₂ saturated KOH 0.1 M for Pt 10% impregnated on doped sample compared to Pt/C 20 wt.%

Moreover, LSV curves of the G-STP-900 support and 10% Pt impregnated sample on the rotation rates from 250 to 3500 rpm were measured and number of electrons transferred in the ORR process at potentials ranging from 0.45 to 0.65 (V vs. RHE) were calculated and presented in Fig. 9.

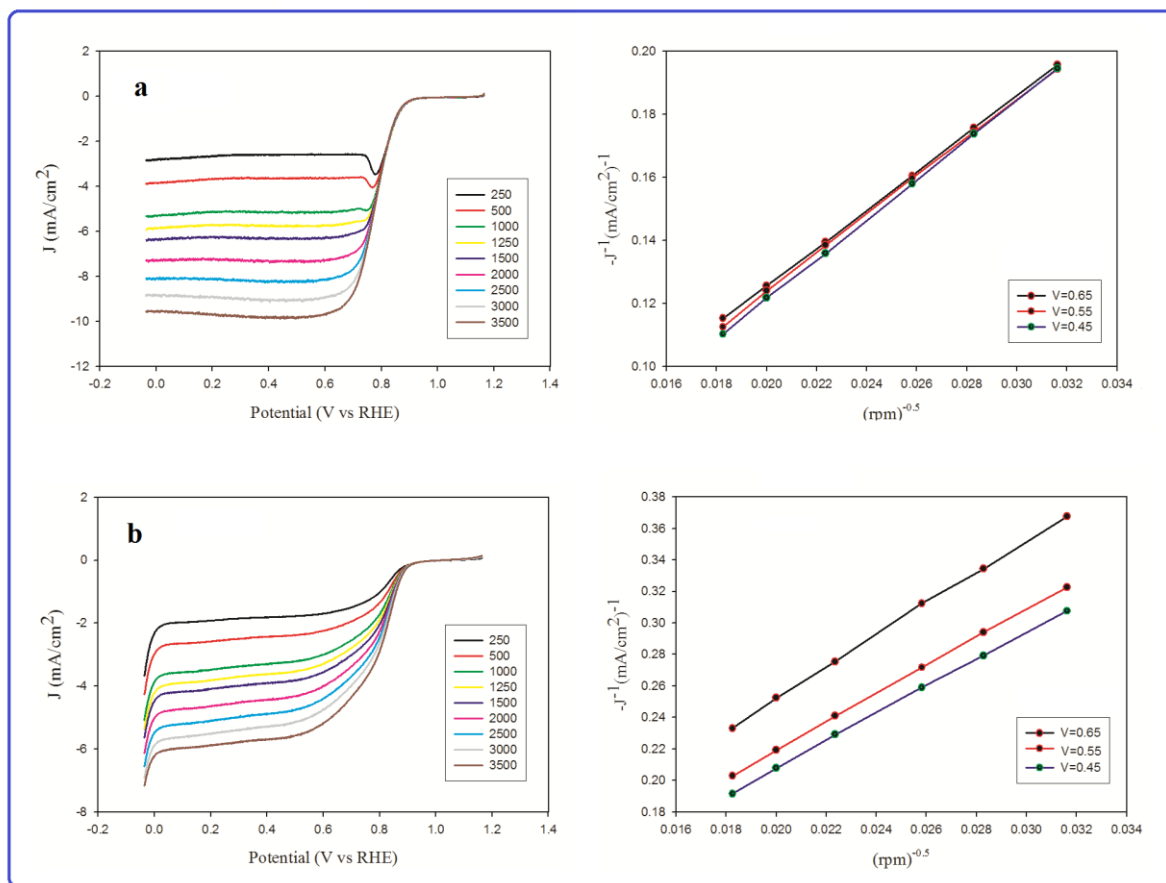


Figure 9. Linear sweep voltammetry at different rotation rate (a) G-STP-900, (b) G-STP-900-Pt 10 in KOH 0.1 M (scan rate 5 mV/s) The corresponding Koutecky–Levich plots at different potentials

Table 4. Comparison of onset potential and electron transfer number of the prepared electrocatalysts

Samples	Electron transfer number (n)	Onset potential (V vs. RHE)
G-STP-900-Pt 10	4.1	1.00
G-STP-900	4.1	0.93
PG-Pt-10	4.0	0.98
PG	2.2	0.85
Pt/C 20 wt%	4.1	0.99

A comparison between onset potential and electron transfer number of G-STP-900-Pt 10 compared to other samples is shown in Table 4.

3.2.3. Microbial Fuel cell test evaluation

Furthermore, the as-synthesized catalysts were evaluated in real MFC. The polarization curves were obtained by changing external resistance (4700, 3900, 3300, 2700, 2200, 1500, 1000, 910, 680, 510, 390 Ω) starting from the open circuit voltage and recording the corresponding voltages at each specified external resistance. Figure 10 represents steady state polarization and power density curves for G-STP-900 and G-STP-900 Pt 10 catalysts in the Microbial fuel cell and the results were compared with PG and Pt /C 20 wt.%.

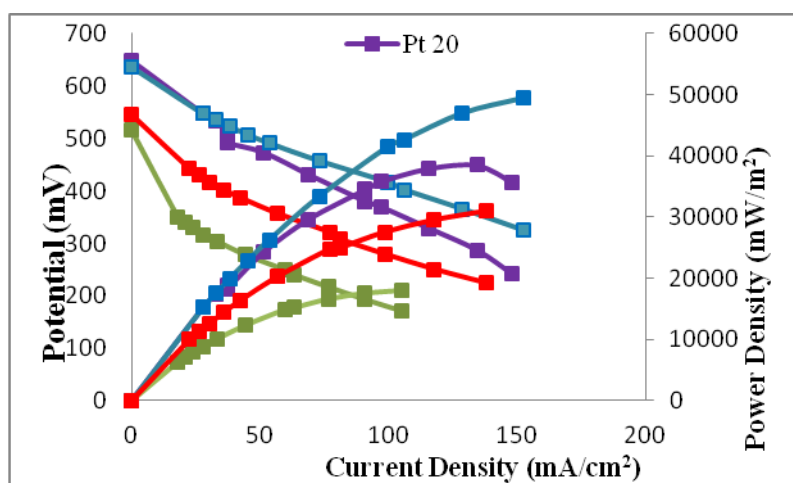


Figure 10. Polarization and power density curves of microbial fuel cell with the prepared cathode catalysts at 25 °C compared to Pt/C 20 wt.%Pt and PG

It is observed that the open circuit potential of the fuel cell with G-STP-900, G-STP-900 Pt 10, PG and Pt/C were 545, 637, 515 and 640 mV, respectively. Due to the high ORR electrocatalytic activity of the optimal prepared sample, the microbial fuel cell with G-STP-900 Pt 10 cathode yields a high peak power density of 49717 mW/m^2 , which is much higher than that of for the PG (18028 mW/m^2) and Pt/C 20 wt.% (38631 mW/m^2) cathodes implying the remarkable performance of this electrode. Also, the G-STP-900 Pt 10 sample shows much higher power density than Pt/C 20 wt.% indicating the important effect of heteroatom doped on carbon substrate. According to the obtained results, the using 10% Pt on the heteroatom doped graphene (49717 mW/m^2) Leads to MFC performance enhancement in comparison with 20 % Pt/C (38631 mW/m^2). Consequently, because of the supporting role, impregnation of the 10% Pt on the N,S co-doped graphene seems to be the optimal catalyst in this research (G-STP-900 Pt 10). Therefore, by decreasing the Pt amounts from 20 to 10%, due to simultaneous doping of S and N in carbon structure and their synergetic effects, the number of active sites could be increased and catalyst performance boosted. Hence, it could be an attractive candidate as MFC cathode catalyst, which increased the performance, but by less Pt amounts.

4. CONCLUSION

In this work, nitrogen-sulfur co-doped on the porous graphene catalysts was successfully prepared via pyrolysis method. Moreover, the effect of Pt impregnation on ORR was investigated. The results showed that the impregnated S, N co-doped graphene catalyst by 10% Pt presented a comparative ORR performance respect to Pt/C 20wt%. The onset of optimum catalyst was 1.00 V vs. RHE which is higher than Pt/C 20wt.% (0.99 V vs. RHE). Furthermore, the optimized catalyst (G-STP-900 Pt 10) conducts ORR in $4e^-$ transfer pathway. Therefore, the optimal prepared electrocatalyst with lower amount Pt instead of Pt/C 20wt.% catalyst, can be a good candidate for oxygen reduction reaction in low-temperature microbial fuel cells.

ACKNOWLEDGEMENTS

The authors thank the Research Council of University of Tehran and the Research Institute of Petroleum Industry for the financial support of this work.

References

1. H. Han, N. Parveen. S.A. Ansari and M.H. Cho, *RSC Advances*, 6 (105) (2016)103446-103454.
2. Y. Li, W. Zhou, H. Wang, L. Xie, Y. Liang, F. Wei, S.J. Pennycook and H. Dai, *Nature Nanotechnology*, 7 (2012) 394–400.
3. H.W. Liang, X. Cao, F. Zhou, C.H. Cui, W.J. Zhang and S.H. Yu, *Adv. Mater.*, 23 (2011) 1467–1471.
4. D.H. Kwak, Y.W. Lee, S.B. Han, E.T. Hwang, H.C. Park, M.C. Kim and K.W. Park, *J Power Sources*, 275 (2015) 557–562.
5. H. Zhang, Y. Wang, D. Wang, Y. Li, X. Liu, P. Liu, H. Yang, T. An, Z. Tang and H. Zhao, *small*, 10 (16) (2014) 3371–3378.
6. S. Bag, B. Mondal, A. K. Das and C. R. Raj, *Electrochimica Acta*, 163 (2015) 16–23.
7. Y. Qiu, J. Huo, F. Jia, B.H. Shanks and W. Li, *J. Mater. Chem. A*, 4 (2016) 83-95.
8. N. Alexeyeva, E. Shulga, V. Kisand, I. Kink and K. Tammeveski, *Journal of Electroanalytical Chemistry*, 648 (2010) 169–175.
9. Qiliang Wei , Xin Tong, Gaixia Zhang , Jinli Qiao , Qiaojuan Gong and Shuhui Sun, *Catalysts*, 5(3) (2015) 1574-1602.
10. L. Samiee, S. Sadegh Hassani, M.R. Ganjali and A. M. Rashidi, *Iranian Journal of Hydrogen & Fuel Cell*, 3 (2017) 231-240.
11. Z. Lin, G.H. Waller, Y. Liu, M. Liu and C.P. Wong, *Carbon.*, 53 (2013) 130-136.
12. B. Wang, L. Si, J. Geng, Y. Su, Y. Li, X. Yan and L. Chen, *Applied Catalysis B: Environmental*, 204 (2017) 316-323.
13. F. Razmjooei, K.P. Singh, M.Y. Song and J.S. Yu, *Carbon*, 78 (2014) 257–267.
14. X. K. Kong, Z.Y. Sun, M. Chen, C.-L. Chen, and Q.W. Chen, *Energy & Environmental Science*, 6 (2013) 3260-3266.
15. Z. Lin, G. Waller, Y. Liu and C.P. Wong, *Nano Energy*, 2(2) (2013) 241–248.
16. D. Guo, R. Shibuya, C. Akiba and J. Nakamura, *Science*, 351 (6271) (2016) 361-365.
17. Wu Z.S. Wu, S. Yang, Y. Sun, K. Parvez, X. Feng and K. Mullen, *J. Am. Chem. Soc.*, 134 (2012) 9082-9085.
18. A.M. Rashidi, Alimorad, L. Mahmudian and H. Dehghani, *US Patent*, 20160060123, 2016.
19. S. Sadegh Hassani. M.R. Ganjali, L. Samiee, A.M.Rashidi, S.Tasharrofi, A.Yadegari, F.Shoghi and R.Martel, *J. Nanoscience and nanotechnology*, 18 (2018) 4565–4579.

20. L. T. Qu, Y. Liu, J.B. Baek and L.M. Dai, *ACS Nano*, 4 (2010) 1321–1326.
21. A. Ziaedini, H. Rashedi, E. Alaie and M. Zeinali, *fuel cell*, DOI: 10.1002/fuce.201800027.
22. G. Jo, J. Sanetuntikul and S. Shanmugam, *RSC Adv*, 5(2015) 53637-53643.
23. M.A. Patel, F. Luo, M. R. Khoshi, E. Rabie, Q. Zhang, C.R. Flach, R. Mendelsohn, E. Garfunkel, M. Szostak and H. He, *Nano*, 10 (2)(2016) 2305–2315.
24. G. Panomsuwan, N. Saito and T. Ishizaki, *ACS Appl. Mater. Interfaces*, 8 (11) (2016) 6962–6971.
25. Z. Sun, J. Masa, P. Weide, S.M. Fairclough, A. W. Robertson, P. Ebbinghaus, f.H. Warner, S.C.E. Tsang, M. Muhlerb and W. Schuhmann, *J. Mater. Chem. A*, 3 (2015) 15444-15450.
26. Y. Su, Y. Zhang, X. Zhuang, S. Li, D. Wu, F. Zhang and X. Feng, *Carbon*, 62 (2013) 296– 301.
27. H. Lin, L. Chu, X. Wang, Z. Yao, F. Liu, Y. Ai, X. Zhuang and S. Han, *New J. Chem.*, 40 (2016) 6022-6029.
28. Z. Xing, Z. Ju, Y. Zhao, J. Wan, Y. Zhu, Y. Qiang and Y. Qian, *Scientific Reports*, 6 (2016) 26146.
29. C.B. Ma, Z.T. Zhu, H.X. Wang, X. Huang, X. Zhang, X. Qi, H.L. Zhang, Y. Zhu, X. Deng, Y. Peng, Y. Hand, H. Zhang and L. Lu, *ACS Appl. Mater. Interfaces*, 7 (2) (2015) 1207–1218.

© 2018 The Authors. Published by ESG (www.electrochemsci.org). This article is an open access article distributed under the terms and conditions of the Creative Commons Attribution license (<http://creativecommons.org/licenses/by/4.0/>).